Journal of Dentistry 110 (2021) 103688

Contents lists available at ScienceDirect

Journal of Dentistry

journal homepage: www.elsevier.com/locate/jdent

A novel non-destructive technique for qualitative and quantitative measurement of dental erosion in its entirety by porosity and bulk tissue-loss

Mathew J.F. Hookham [a,*], Richard J.M. Lynch [b], Declan P. Naughton [a]

[a] School of Life Science, Pharmacy and Chemistry, Kingston University London, United Kingdom
[b] Department of Health Services Research and School of Dentistry, University of Liverpool, United Kingdom

ARTICLE INFO

Keywords:
Erosion
Enamel
Confocal
Profilometry
ICP-AES
Mineral loss

ABSTRACT

Objective: To explore the potential of combining non-contact profilometry (NCP) and confocal laser scanning microscopy (CLSM) data to measure the entire erosive process non-destructively and to validate findings using inductively coupled plasma-atomic emission spectroscopy (ICP-AES), scanning electron microscopy (SEM) and surface microhardness (SMH) using the same samples throughout.

Methods: Polished bovine enamel samples (n = 35) were divided into groups (7/group) with similar SMH values. Samples underwent individual erosive challenges (1 % citric acid, pH3.8) for 1, 5, 10, 15 or 30 min under stirring and aliquot extracts were analysed for Ca and P by ICP-AES. SMH was used to measure erosive softening. Profilometry was used to assess bulk volume loss (BVL). Images were captured by SEM. Samples were stained with rhodamine-B (0.1 mM, 24 h) and images captured by CLSM. Image processing was used to determine changes in fluorescent volume for the first 10 μm (ΔFV_{10}) for each enamel sample which were combined with BVL to calculate total lesion volume (TLV). ANOVA, linear regression and Pearson correlation analysis were used where applicable.

Results: Surface softening, [Ca], [P], BVL and $\Delta FV_{10\mu m}$ increased with acid erosion duration which were significant by 10 min ($P < .01$). The Ca:P ratio increased to 1.57 then decreased after 5 min erosion suggesting a sub/surface phase change, which was observed by SEM and CLSM showing significant changes to the enamel surface and subsurface morphology with time. Combination of BVL and ΔFV_{10} as TLV strengthened the significant correlations with [Ca], [P], and SMH ($P < .01$).

Conclusion: This novel combination of CLSM and NCP allows for concurrent non-destructive quantification of the entire erosive process by mineral loss, and qualitatively characterise microstructural changes during dental erosion.

1. Introduction

Dental erosion is considered a surface phenomenon caused by exposure to acid of non-bacterial origins, in contrast to dental caries [1–7]. Dental erosion progresses by the combination of bulk surface loss and mineral-loss below the surface (subsurface) from the erosive lesion [1]. Bulk surface loss during erosion can be quantified with relative ease using profilometric techniques [8,9]. Therefore, erosive lesions are typically measured using direct surface changes, being the characteristic bulk tissue loss (profilometry) or surface softening (surface microhardness, SMH) [10,11]. Measurement of these surface changes are useful for quickly assessing the extent of erosion without destructive sample preparations and are routinely used to assess anti-erosive properties of oral care products [8–17]. However, erosive lesions, while don't penetrate the subsurface as deep as carious lesions, nonetheless have a subsurface component often overlooked. The available techniques for subsurface characterisation are limited with little or no information provided on pore morphology of the erosive lesion. Currently no method exists which can assess the surface and subsurface non-destructively, qualitatively or quantitatively, for changes in pore morphology of an erosive lesion.

Transverse microradiography (TMR), which is widely regarded as

* Corresponding author at: School of Life Science, Pharmacy and Chemistry, Kingston University London, Penrhyn Road, Kingston Upon Thames, KT1 2EE, United Kingdom.
E-mail address: K1112053@kingston.ac.uk (M.J.F. Hookham).

https://doi.org/10.1016/j.jdent.2021.103688
Received 9 February 2021; Received in revised form 11 April 2021; Accepted 1 May 2021
Available online 5 May 2021

the gold standard for measuring mineral loss as a function of depth for carious lesions, has seen limited use with erosive lesions [18–20]. It is destructive and extremely difficult to perform on the fragile erosive lesion surfaces and provides no information on the pore morphology.

Scanning electron microscopy (SEM) was utilised by Fowler et al. [19] in a similar fashion as TMR where improvements in the resolution, attributed with SEM, provided pore morphology information of the subsurface (as well as mean mineral density distribution), although only on the prepared surfaces of sections, assumed to be representative of the entire lesion. Again, this is a destructive technique.

Optical coherence tomography (OCT) is a non-destructive means of imaging the surface and subsurface by the scattering of light which has seen success primarily with caries lesions. Use of OCT with erosive lesions has been explored with limited success, but lacks the spatial resolution for the study of pore morphology [21–25].

Inductively coupled plasma atomic emission spectroscopy (ICP-AES) estimates erosion progression via changes in the Ca and PO_4 concentrations of experimental solutions, using calculations based on hydroxyapatite stoichiometry and density [8,26–28]. However, there is currently no way to distinguish between surface and subsurface Ca and PO_4 eluted during erosion meaning this method measures total erosive damage indirectly.

Non-contact profilometry (NCP) is capable of non-destructive analysis of bulk tissue loss of the enamel surface something which is routinely used to measure erosion *in vitro* [12–17] and *in situ* [9,17]. Coupling of profilometry with sonication allowed for the erosive lesion to be assessed from differences in height after removal as reported Eisenburger et al. [29]. This coupling of profilometry and sonication creates a potentially destructive method of assessing the depth of the erosive lesion which is not guaranteed to be removed entirely.

Techniques which encompass both areas of erosion (bulk tissue and subsurface mineral loss) are few, as previously discussed by Hookham et al. [30], with the majority requiring destructive sample preparation or have limited sensitivity, such as NCP, TMR, SEM and OCT [18,19,25]. Meaning a viable technique, or combination, which can assess both areas non-destructively is needed.

Confocal laser scanning microscopy (CLSM) on the other hand is capable of non-destructive assessment of erosion as a function of depth by fluorescent volume quantified using image processing, as reported by Hookham et al. [30]. Using image processing with CLSM allows for further understanding of the stages of erosion at the subsurface in which a steady state of erosion (SSE) being reached was shown not to occur after 30 min exposure to citric acid [30]. It is also a technique which has been correlated with mineral loss from caries lesions measured by TMR [31] showing the validity of using CLSM to measure subsurface demineralisation.

Using NCP and CLSM together to measure the erosive process entirely and in its parts (surface/ subsurface) has yet to be reported as an entirely non-destructive method. Therefore, this study extends previous work reporting the application of a novel image processing method of CLSM compared against a multitude of applications being SMH and NCP [30]. The key aim of this study is to build upon previous work by Hookham et al. [30] exploring the potential to combine profilometric and CLSM data for measuring the entire erosive process non-destructively and validate findings using ICP-AES, SEM and SMH using the same samples throughout. A secondary aim was to determine the reproducibility/comparability of the image processing method meaning replication of certain experimental approaches from a previous study [30] was necessary to serve as a comparator.

2. Methods

2.1. Sample preparation

Bovine enamel samples were prepared as previously reported by Hookham et al. [30] with differences outlined below. One enamel sample was imbedded per resin disc with a rough area $\approx 0.5 \pm 0.2$ cm^2. Acid resistant varnish was placed on the surface of the disc leaving an exposed area of enamel roughly 0.1 cm^2 (Fig. 1). The area was measured from a photograph of the sample against a ruler to calibrate the pixel dimensions using Fiji (Image J, Ver.1.52i).

2.2. Experimental procedure

Thirty-five enamel blocks (n = 7/group) were allocated at random to one of five erosion period groups (1, 5, 10, 15 and 30 min) so no significant difference in mean microhardness or exposed area were detected. Samples were individually acid etched in 100 mL of citric acid (0.05 M, pH 3.8 adjusted with KOH) under agitation using a stirrer bar hot plate (Stuart Hotplate Stirrer SB302) set at ≈150 rpm. Samples were removed and rinsed with DI water for 10 s and left to air dry. A 20 mL acid aliquot was kept from each sample acid solution and analysed by ICP-AES immediately. SMH was carried out prior to acid resistant varnish removal by acetone then subsequently followed by SEM, NCP and CLSM.

2.3. Surface microhardness

A Vickers surface microhardness indenter (Struers Duramin 1, Ver.2.01) was used to measure enamel hardness using a constant load (1.98 N) and 10 s dwell time. The objective lens (40x, NA 0.65) was zero set and calibrated to a known standard (400 kg mm^{-2}) using the test parameters prior to analysis. The samples were measured 6 times for a mean surface hardness value before (SMH_b) and after erosion (SMH_e), with change in hardness (ΔSMH) being calculated by subtracting mean erosion hardness from mean baseline hardness values ($SMH_b - SMH_e = \Delta SMH$).

2.4. Inductively coupled plasma-atomic emission spectroscopy

ICP-AES (Jobin-Yvon, Ultima 2 ICP-AES) analysed Ca and P content of acid solutions using spectral lines 393.366 and 213.618 nm respectively. A calibration curve was created with an acceptable correlation value (R = 0.999) using known standards of 5 and 10 ppm Ca and P respectively within the same solution. The test solutions were tested from blank acid and increasing in erosion duration (1–30 min), measuring in triplicate per test solution. The amount of each element was converted to a concentration and normalized to the area of exposed enamel. The background levels of Ca and P measured in the blank acid was subtracted from all test samples [26,27] .

2.5. Non-contact white light profilometry

3D non-contact profilometry (Scantron, Proscan 2000, sensor S13/ 1.1) was utilized after erosion. A raster scanning pattern with a 50-μm step in the x and y directions measured the entire sample with a lateral resolution of 25 nm. An average of 8 scans was collected with a sampling rate of 100 Hz. Using the dedicated Scantron software (Proscan V2.1.1.15B) step height was measured after using 3-point levelling of the reference surface to account for any unevenness in flatness of the samples. The average height of the data inside a consistent measurement area 10 μm either side of the step formed from erosion was measured, where the difference between the eroded and reference zones average height was deemed the step height. Step height was averaged over 3 measurements per sample. The mean step height collected was determined to be the net bulk tissue loss of the sample. Bulk volume loss (BVL) was calculated by multiplying the step height by the known area measured by CLSM (4031 μm^2).

2.6. Scanning electron microscopy

SEM (Phenom G2 Pro) was used to capture images of exposed enamel

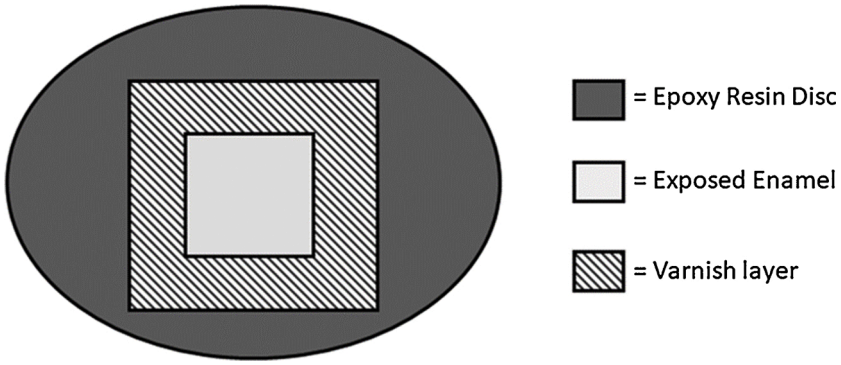

Fig. 1. Schematic of single block sample preparation.

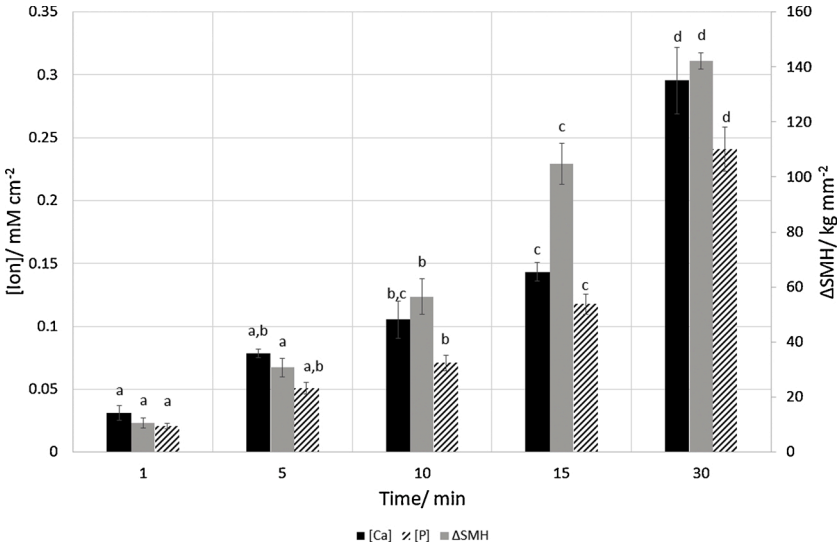

Fig. 2. Mean change in surface microhardness (ΔSMH) of bovine enamel and mean eluted calcium and phosphorus concentrations after exposure to stirred citric acid (1 %, pH .8) solutions for different durations (1, 5, 15, 30 min) (n = 7/ group) measured by surface microhardness and inductively coupled plasma-atomic emission spectroscopy. Error bars are standard errors of the mean. Significant Pearson values of 0.937, 0.917 and 0.948 for ΔSMH, [Ca] and [P] respectively ($P < .01$). Different lowercase letters denote significant differences between time points ($P < .05$).The ΔSMH data presented are reproduced using the same experiment protocol as reported by Hookham et al. [30] to serve as a same sample set comparison.

surfaces, at different magnifications (1000×, 12000×), after the experimental conditions. SEM was used in back scattered detection mode with an accelerating voltage of 10 kV. Working distance and beam spot size were adjusted automatically by dedicated phenom software to achieve a resolution of 25 nm. The images were compared to determine morphological changes to the surface as erosion progressed.

2.7. Confocal laser scanning microscopy

Rhodamine B (aq, 0.1 mM, pH 8) was used to stain enamel samples for 24 h within a fridge at 8 °C in total darkness to prevent photobleaching. After staining and rinsing with DI water for 10 s the samples were then mounted onto a glass slide (No. 1.5) with an immersion oil (Olympus immersion oil Type-F, MOIL-30). Images where captured using an inverted confocal laser scanning microscope (Olympus Fluo View FV1000, FV10-ASW Software Ver.4.1.1.5) in fluorescence mode with an oil immersion lens (Zeiss ACHROPLAN, 100x, NA 1.25). A 543 nm laser (HeNe-G/ Helium-Neon gas laser) set at 49 % intensity was used to excite rhodamine B, where an emission spectrum was captured between 555–655 nm. Each pixel was scanned at a rate of 10 µs across a window of 800:800 pixels with zoom set at 2, resulting in a voxel size of 0.079 (x) x 0.079 (y) x 0.450 (z) µm. Gain (2) and offset (8) were kept constant throughout all imaging with adjustment to brightness made by fine-tuning the detector voltage. A pinhole of 246 µm was employed by the software automatically.

2.8. Image processing

Fluorescent volumetric data was acquired using image processing with Fiji (Image J, Ver.1.52i) as previously reported by Hookham et al. [30]. The sample image was loaded into Image J as a 12-Bit image. A sliding parabola algorithm with pixel size 25 was used to subtract the background and reduce any uneven illumination of the sample. A 3D median filter was applied with a size of 2 × 2 × 2 pixels to reduce noise while preserving object edges. A local contrast enhancement was performed with block size (10 pixels) increasing the histogram binning. The image was segmented using Huang's automatic threshold to separate objects (fluorescent dye) and background pixels creating a binary image using the stack histogram. The foreground and background pixels/voxels were measured for each image within a stack where area was calculated using the known pixel dimensions. The area fraction as a function of depth was then determined for every sample and plotted in Excel.

A defined surface was used to align the fluorescent area as a function of depth data allowing for averages to be calculated at each depth. Fluorescent volume as a function of depth was calculated using area under the curve analysis. The mean change in fluorescent volume (ΔFV) was calculated by subtracting the volumetric data of a reference image from the data of an eroded image of from the same sample. The data were subsequently averaged and plotted as a function of depth. ΔFV was determined for the first 10 µm of each enamel sample and subsequently averaged for each group (ΔFV_{10}). Total lesion volume (TLV) was

estimated by the addition of BVL and ΔFV_{10}.

2.9. Statistical analysis

Using a dedicated statistical packaged (IBM SPSS, Ver26) 2-way ANOVA and Tukey post hoc tests were used to determine significant differences in mean ΔSMH, BVL, [Ca], [P], ΔFV and TLV between different erosion durations ($P < 0.05$). Pearson correlations were calculated between measured variables and tested for significance in SPSS ($P < 0.01$). Linear regression analyses were performed within Excel.

3. Results

This work extends data previously reported [30] on the novel application of image processing of CLSM images and compared to SMH and NCP data, to this end similar data was collected in this study for comparison.

3.1. Surface microhardness and acid Ca and PO_4 analysis

Mean surface microhardness values and exposed surface areas did not differ significantly at baseline ($P > .56$). After exposure to acid all samples hardness values reduced significantly from baseline ($P < .002$), with a total reduction of 55 % by 30 min. Fig. 2 shows the mean change in surface microhardness (ΔSMH) of the enamel surface as erosion progressed. ΔSMH was shown to significantly increase with duration of erosion by 10 min ($P < .014$). A linear trend is maintained until 30 min where a plateau in softening is detected. A significant positive correlation is detected between erosion duration and ΔSMH with a Pearson value of 0.937 ($P < .01$). Fig. 2 shows the progression of erosion by Ca and P concentrations eluted into the acid solutions which increase with increasing duration of erosion. A significant effect of erosion was detected on the [Ca] and [P] ($P < .001$). A significant positive correlation was detected between concentration of eluted Ca or P and erosion duration with Pearson values of 0.917 and 0.948 respectively ($P < .01$). The Ca:P ratios in Table 1 increased to 5 min then decreased thereafter.

Table 1
Inductively coupled plasma-atomic emission spectroscopy results of calcium and phosphorus concentrations with estimated lesion depth (LD) for bovine enamel exposure to stirred citric acid (1 %, pH 3.8) solutions for different durations (1, 5, 10, 15, 30 min).

Erosion Duration/min	[Ca]/mM cm^{-2} (SE)	[P]/mM cm^{-2} (SE)	Ca:P (SE)
1	0.0309 $(0.00585)_a$	0.0208 $(0.00229)_a$	1.44 (0.12)
5	0.0783 $(0.00342)_{a,b}$	0.0508 $(0.00446)_{a,b}$	1.63 (0.19)
10	0.105 $(0.0149)_{b,c}$	0.07106 $(0.00619)_b$	1.45 (0.078)
15	0.143 $(0.00744)_c$	0.118 $(0.00790)_c$	1.23 (0.023)
30	0.295 $(0.0266)_d$	0.241 $(0.0176)_d$	1.21 (0.032)

a, Different lower-case letters denote significant differences between groups ($P < .05$).

3.2. Confocal laser scanning and scanning electron microscopy

The reference image shown in Fig. 3 shows an intact enamel surface with scratches formed by the polishing procedure during sample preparation. Erosion for 1 min led to no distinct visual surface or orthogonal changes being observed by CLSM or SEM. After 5 min erosion the surface was observed to change by CLSM showing visible prism structures and a rougher surface which was more distinct by 30 min erosion with the gradual removal of the surface scratches from sample preparation. Comparing the orthogonal view, an increase in rhodamine B fluorescence (light grey) was detected with increasing erosion duration, indicating the lesion beneath the surface was growing in depth. The pore architecture was observed to increase in size becoming increasingly more visible with time spent exposed to acid. The SEM micrographs at 1000 and 12000× magnifications confirm what was observed by CLSM with increasing roughness and exposure of the prism structures as erosion progressed with time. The enamel surface was shown to be heavily eroded after 10 min erosion by SEM.

3.3. Confocal laser scanning microscopy and non-contact profilometry volumetric analysis

Fig. 4 shows a significant ($P < .001$) increase in volume loss with duration exposed to acid from the surface (BVL), inside the erosive lesion (ΔFV_{10}) and their combination (Total lesion volume, TLV). Significant differences in durations times for BVL, ΔFV_{10} and TLV were detected by 10 min ($P < .01$). Linear regression analysis of Fig. 4 showed a rate of BVL, ΔFV_{10} and TLV of 5509, 4155 and 9664 $\mu m^3\ min^{-1}$ respectively. A strong linear correlation with time was also detected for BVL, ΔFV_{10} and TLV by Pearson values of 0.904, 0.803 and 0.848 respectively ($P < .01$).

3.4. Correlations

Table 2 shows the Pearson correlation values between measured variables. A strong correlation exists between [Ca] and [P] concentrations ($R = .982$). The combination of two variables to create TLV (BVL + ΔFV_{10}) was shown to increase the strength of the correlation with hardness and ion concentrations ($R > .866$). All correlations were determined to be significant ($P < .001$).

4. Discussion

This report of the novel combination of CLSM and profilometry volume measurements extends the previous results [30] where CLSM was applied to the same experimental model, facilitating for comparisons between the results. The CLSM based measurements were reproducible across both papers, with a minor change to the image processing method introducing a 3D median filter to enhance noise reduction. Use of citric acid, bovine substrate and rhodamine B were suitable for the nature of this work as discussed previously by Hookham et al. [30]. This development allows for a non-destructive approach whereby combination of CLSM and profilometry data provide quantitative and qualitative assessment of dental erosion at the surface/subsurface.

The findings of increasing surface softening (Fig. 2) and bulk volume loss (Fig. 4) support the rapid progression of erosion, which agreed with the results reported by Hookham et al. [30]. A steady state of erosion could be suggested due to the rate of softening reducing with time as measured by SMH. The SSE is suggested to occur when the rate of lesion progression and bulk tissue loss reach equilibrium, where the lesion does not appear to grow in depth meaning softening remains constant as suggested by Lussi et al. [32] and Shellis et al. [33]. The CLSM and ICP-AES results show a contrasting response with no SSE being achieved with continuous lesion growth and mineral loss detected (Figs. 2 & 4). CLSM cross sectional images showed consistent lesion growth in depth as erosion progressed (Fig. 3), evidencing the absence of SSE.

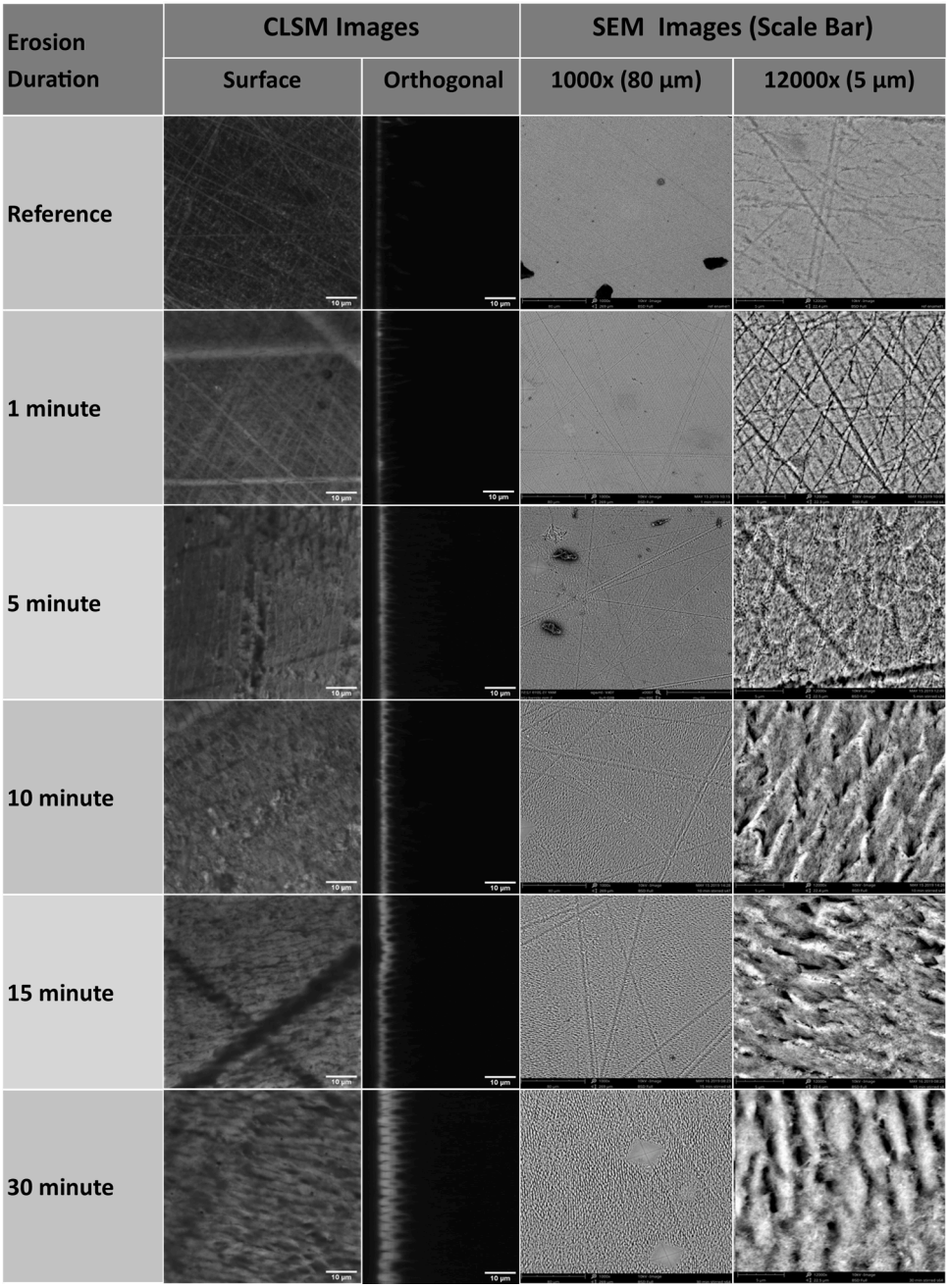

Fig. 3. Scanning electron microscopy micrographs of a bovine enamel surface exposed to different durations (1, 5, 10, 15, 30 min) of stirred citric acid (1 %, pH 3.8) solutions at 1000× and 12000× magnifications with scale bars of 80 and 5 µm respectively. Confocal laser scanning microscopy images of surface and cross sections of bovine enamel stained with rhodamine B for 24 h after different durations exposed to citric acid (1 %, pH 3.8) solutions. Scale bars are 10 µm.

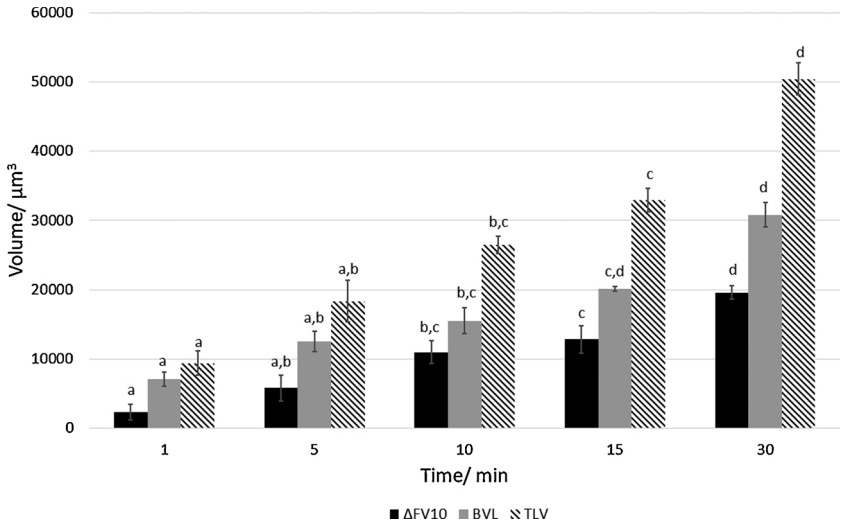

Fig. 4. Average bulk volume loss (BVL), total fluorescent volume (ΔFV_{10}) and total lesion volume (TLV) of bovine enamel exposed to stirred citric acid (1 %, pH 3.8) solutions for different durations (1, 5, 10, 15, 30 min) (n = 7/ group). Error bars are standard errors of the mean. Pearson values of 0.904, 0.803 and 0.848 for BVL, ΔFV_{10} and TLV respectively ($P < .01$). Different lowercase letters denote significant differences between time points ($P < .05$).

Table 2
Variable Vs Variable Pearson Correlation Table.

Measurement	Pearson Value	Measurement	Pearson Value
[Ca] Vs ΔSMH	0.850*	[P] Vs ΔSMH	0.884*
[Ca] Vs BVL	0.841*	[P] Vs BVL	0.878*
[Ca] Vs ΔFV_{10}	0.766*	[P] Vs ΔFV_{10}	0.774*
[Ca] Vs TLV	0.866*	[P] Vs TLV	0.892*
[Ca] Vs [P]	0.982*	ΔSMH Vs ΔFV_{10}	0.835*
ΔSMH Vs TLV	0.910*	ΔSMH Vs BVL	0.858*
BVL Vs ΔFV_{10}	0.753*		

ΔSMH = Change in surface microhardness, ΔFV_{10} = Change in fluorescent volume.
BVL = Bulk volume loss, TLV = Total lesion volume.
* Denotes significant correlations at $P < .01$ two tailed (n = 35).

The variation in findings between SMH and CLSM may arise from a lack of sensitivity of SMH indentation relative to more subtle erosive damage at greater depths, which was captured by CLSM. The main contributing factor to the reduced sensitivity of SMH at measuring erosion is the penetration depth of the indenter which is limited (≈5 µm) causing any erosive damage below this value to be largely unaccounted for. Comparable conclusions of caries lesions upon lamination of the lesion surface have been drawn for SMH [34]. CLSM can be used to assess the erosive lesion with greater sensitivity in depth compared to SMH leading to the increased understanding of the erosive process established within this study.

The CLSM surface images show a gradual change in the enamel surface morphology from smooth to a rougher enamel surface which was also detected by SEM micrographs (Fig. 3). The SEM micrographs show the distinct progression of erosion with time by the removal of bulk tissue exposing the prism morphology at the surface, whereby distinct tissue loss is observed after 5 min erosion. After 5 min erosion the prism boundaries are heavily eroded agreeing with BVL measured by profilometry. The SEM shows the surface becoming rougher as erosion progressed which is typical of the polished enamel substrate used which deviates from a natural unpolished enamel surface which became smoother, as shown by Mullan et al. [35] using human enamel.

ICP-AES was used to detect the rapid dissolution of Ca and PO_4 during erosion, whereby at 5 min the enamel was eroding entirely with a Ca:P ratio like that of intact enamel 1.61 [36] (Table 1). As erosion progressed the Ca:P ratio reduced in solution, indicating a possible reprecipitated phase onto the enamel surface with a Ca:P ratio closer too other calcium phosphate minerals (Brushite, Monetite, Whitlockite) [37,38]. While the acid solution would be infinitely undersaturated with respect to relevant calcium phosphates, localisation of dissolution products at the enamel-acid interface may lead to supersaturation. This could lead to localised supersaturation and deposition of these $CaPO_4$ onto the enamel surfaces as results of the demineralisation as is for the case for dental caries [39,40]. Lynch et al. [40] shows that remineralisation is also possible at low pH, albeit in the presence of fluoride. Gao et al. [39] showed demineralisation was completely inhibited at pH 2.5 where the degree of saturation of the demineralisation solutions was shown to be crucial.

The potential formation/deposition of a more acid resistant material could explain the reduction in Ca:P ratio (to 1.21) alongside the rates of BVL and softening. It is well known that acidic calcium phosphates, like brushite, have a lower solubility than hydroxyapatite under acidic conditions (pH < 4) [41,42]. The increased resistance to acid dissolution would drive the acid to penetrate deeper into the enamel and remove more acid soluble material, something observed with dental caries [2,40,43,44], explaining the steady increase in lesion volume with depth captured and measured by CLSM (supplement file, Figs. 1 & 2). The differences in the ΔFV depth profiles of erosive lesions of varying severity was like that reported by Hookham et al. [30], where lesion growth was detected as a function of depth showing the reliability of this CLSM measurement technique. The inability to determine Ca and P origins (surface/subsurface) measured by ICP-AES means further compositional analysis, such as secondary ion mass spectrometry or X-ray photoelectron spectroscopy, would be required to identify the deposition of less soluble material.

The combination of BVL and ΔFV_{10} (as TLV) allowed for erosion to be measured entirely non-destructively something which has yet to be reported to this authors knowledge. TLV was shown to increase the Pearson correlation values with both Ca and PO_4 when compared to BVL or ΔFV_{10} alone (Table 2). This increase in Pearson value would be expected as Ca and PO_4 would originate from mineral removed from both the surface and internal surfaces, and so give a total picture of the erosive process. It has been shown that applying image processing to CLSM images to quantify subsurface erosion by ΔFV_{10} and combining this with bulk tissue loss is a viable method for assessing erosion in its entirety, something which has not been reported before. This image processing method allows for greater insights into the erosive process showing the effects beneath the surface are more important than

previously considered.

Utilising image processing of CLSM with NCP allowed for the novel combination of metrics as TLV allowing for the entire erosive process to be quantified non-destructively. The combination of metrics as TLV strengthened the correlation with Ca and P measured by ICP-AES further showing the validity of this measurement approach for assessing dental erosion. The resolution of CLSM is lower than that of SEM but is more than adequate for imaging pore spaces of 50–200 nm. This CLSM resolution allows for changes in pore morphology to be visualized and quantified which is a clear improvement over TMR and OCT. The non-destructive nature of CLSM also makes this method a viable technique for assessing multiple locations of the enamel subsurface something which TMR and SEM are unable once sectioned. Upon coupling NCP with CLSM a total picture of the erosive process was achieved further showing no steady state of erosion was detected by the constant lesion growth with depth, supporting previous findings reported by Hookham et al. [30].

This shows that the data from two different studies is comparable making the CLSM and NCP a valid and powerful approach for measuring erosion. This comparability is further enhanced by the high accessibility of CLSM, NCP and ImageJ, with most research institutes having access to these common techniques and software. It should also be noted that CLSM is also capable of measuring bulk volume loss meaning it is possible to measure erosion entirely non-destructively with one technique [15,45,46]. This means if access to NCP is limited CLSM can be utilised in its place increasing accessibility further.

Limitations of using this method are the errors associated with measuring small step height changes with NCP, which was shown to increase significantly when measuring height changes below 0.49 μm by Mullan et al. [47]. This means limited damage from initial erosion maybe difficult to measure using NCP. A limitation associated with CLSM is the measurements for exposed and reference areas are not the same location and, like TMR, assumes they would react in the same way. Furthermore, no direct compositional analysis can be achieved with either NCP or CLSM meaning other methods would be needed to identify exactly any potential phase changes during the erosive process at the enamel surface and subsurface.

Use of human enamel should be explored for optimisation of this method allowing for easier extrapolation of results to a clinical situation. This can be further enhanced by development of a longitudinal method for CLSM and NCP with potential removable or decomposable dyes. This would negate the above limitation and allow for the same sample and location to be imaged from start to finish. This would allow for use in *ex vivo/in situ* clinical studies and if successfully miniaturised a clinical diagnostic tool.

Other areas for improvement of this technique are utilising higher aperture optics and super resolution microscopy to provide enhanced resolution and detail of morphological changes to the enamel surface and subsurface during erosion. Use of more 3D image processing should be explored further to determine if improved segmentation of images and so increasing the accuracy of fluorescent volume measurements by CLSM.

5. Conclusion

This novel approach to capturing and processing CLSM data with profilometric data showed the ability of a new holistic method to measuring mineral loss encompassing the entire erosive process without any destructive sample preparation. Furthermore, this combination strengthened the correlation with other techniques adding value to utilizing these methods together to measure the entire erosive process.

Statement of ethics

Ethical approval was not required due to using sectioned bovine enamel substrate.

Disclosure Statement

Dr Richard J M Lynch was employed by GSK Consumer Healthcare at the time of this study. Dr Mathew J F Hookham has since been employed by GSK consumer healthcare after this study took place. We are not aware of any other conflict of interests.

Funding sources

This work was fully funded by GSK Consumer Healthcare as part of a PhD studentship.

CRediT authorship contribution statement

Mathew J.F. Hookham: Conceptualization, Methodology, Formal analysis, Investigation, Writing - original draft, Writing - review & editing. **Richard J.M. Lynch:** Conceptualization, Methodology, Supervision, Resources, Writing - review & editing. **Declan P. Naughton:** Conceptualization, Methodology, Supervision, Writing - review & editing.

Declaration of Competing Interest

The authors report no declarations of interest.

cknowledgments

The authors acknowledge Simon De Mars for assistance with the ICP-AES analyses.

Appendix A. Supplementary data

Supplementary material related to this article can be found, in the online version, at doi:https://doi.org/10.1016/j.jdent.2021.103688.

References

[1] R.P. Shellis, J.D.B. Featherstone, A. Lussi, Understanding the chemistry of dental erosion, in: A. Lussi, C. Ganss (Eds.), Monogr. Oral Sci. Erosive Tooth Wear From Diagnosis to Ther., 2nd ed., KARGER, Basel, 2014, pp. 163–179, https://doi.org/10.1159/000359943.

[2] C. Robinson, R.C. Shore, S.J. Brookes, S. Strafford, S.R. Wood, J. Kirkham, The chemistry of enamel caries, Crit. Rev. Oral Biol. Med. 11 (2000) 481–495, https://doi.org/10.1177/10454411000110040601.

[3] J.J. Murray, C.R. Vernazza, R.D. Holmes, Forty years of national surveys: an overview of children's dental health from 1973–2013, Br. Dent. J. 219 (2015) 281–285, https://doi.org/10.1038/sj.bdj.2015.723.

[4] J.H. Nunn, P.H. Gordon, A.J. Morris, A. Walker, Dental erosion - changing prevalence? a review of british national childrens' surveys, Int. J. Paediatr. Dent. 13 (2003) 98–105, https://doi.org/10.1046/j.1365-263X.2003.00433.x.

[5] M. Skalsky Jarkander, M. Grindefjord, K. Carlstedt, Dental erosion, prevalence and risk factors among a group of adolescents in stockholm county, Eur. Arch. Paediatr. Dent. 19 (2018) 23–31, https://doi.org/10.1007/s40368-017-0317-5.

[6] R. Moazzez, D. Bartlett, Intrinsic causes of erosion, in: A. Lussi, C. Ganss (Eds.), Erosive Tooth Wear From Diagnosis to Ther., 2nd ed., KARGER, Basel, 2014, pp. 180–196, https://doi.org/10.1159/000360369.

[7] T.S. Carvalho, A. Lussi, Susceptibility of enamel to initial erosion in relation to tooth type, tooth surface and enamel depth, Caries Res. 49 (2015) 109–115, https://doi.org/10.1159/000369104.

[8] N. Schlueter, A. Hara, R.P. Shellis, C. Ganss, Methods for the measurement and characterization of erosion in enamel and dentine, Caries Res. 45 (2011) 13–23, https://doi.org/10.1159/000326819.

[9] T. Attin, F.J. Wegehaupt, Methods for assessment of dental erosion, in: A. Lussi, C. Ganss (Eds.), Erosive Tooth Wear From Diagnosis to Ther., 2nd ed., KARGER, Basel, 2014, pp. 123–142, https://doi.org/10.1159/000360355.

[10] N. Schlueter, L. Neutard, J. Von Hinckeldey, J. Klimek, C. Ganss, Tin and fluoride as anti-erosive agents in enamel and dentine in vitro, Acta Odontol. Scand. 68 (2010) 180–184, https://doi.org/10.3109/00016350903555395.

[11] G.C. de Oliveira, G.P.G. Tereza, A.P. Boteon, B.M. Ferrairo, P.S.P. Gonçalves, T. C. da Silva, H.M. Honório, D. Rios, Susceptibility of bovine dental enamel with initial erosion lesion to new erosive challenges, PLoS One 12 (2017) 1–7, https://doi.org/10.1371/journal.pone.0182347.

[12] D. Dionysopoulos, K. Tolidis, E. Tsitrou, P. Kouros, O. Naka, Quantitative and qualitative evaluation of enamel erosion following air abrasion with bioactive glass

45S5, Oral Health Prev. Dent. 18 (2020) 529–536, https://doi.org/10.3290/j.ohpd.a44689.
[13] S.E. Ainoosah, J. Levon, G.J. Eckert, A.T. Hara, F. Lippert, Effect of silver diamine fluoride on the prevention of erosive tooth wear in vitro, J. Dent. X. 3 (2020) 100015, https://doi.org/10.1016/j.jjodo.2020.100015.
[14] C. Funieru, I.A. Obagiu, R. Oancea, B. Dobrica, R.I. Sfeatcu, M.I. Nicolescu, Erosive potential of three different beverages on human enamel and dentine: an in vitro study, Rev. Chim. 71 (2001) 192–196, https://doi.org/10.37358/RC.20.3.7988.
[15] R.S. Austin, C.L. Giusca, G. Macaulay, R. Moazzez, D.W. Bartlett, Confocal laser scanning microscopy and area-scale analysis used to quantify enamel surface textural changes from citric acid demineralization and salivary remineralization in vitro, Dent. Mater. 32 (2016) 278–284, https://doi.org/10.1016/j.dental.2015.11.016.
[16] A.A. Algarni, F. Lippert, A.T. Hara, Efficacy of stannous, fluoride and their their combination in dentin erosion prevention in vitro, Braz. Oral Res. 29 (2015) 1–5, https://doi.org/10.1590/1807-3107BOR-2015.vol29.0081.
[17] X. Zhao, T. He, Y. He, H. Chen, Efficacy of a stannous-containing dentifrice for protecting against combined erosive and abrasive tooth wear in situ, Oral Health Prev. Dent. 8 (2020) 619–624, https://doi.org/10.3290/j.ohpd.a44926.
[18] B.T. Amaechi, S.M. Higham, W.M. Edgar, Use of transverse microradiography to quantify mineral loss by erosion in bovine enamel, Caries Res. 32 (1998) 351–356, https://doi.org/10.1159/000016471.
[19] C. Fowler, R.J.M. Lynch, D. Shingler, D. Walsh, C. Carson, A. Neale, R.J. Willson, A. Brown, A novel electron-microscopic method for measurement of mineral content in enamel lesions, Arch. Oral Biol. 94 (2018) 10–15, https://doi.org/10.1016/j.archoralbio.2018.06.013.
[20] A.F. Hall, J.P. Sadler, R. Strang, E. de Josselin de Jong, R.H. Foye, S.L. Creanor, Application of transverse microradiography for measurement of mineral loss by acid erosion, Adv. Dent. Res. 11 (1997) 420–425, https://doi.org/10.1177/08959374970110040701.
[21] H.P. Chew, C.M. Zakian, I.A. Pretty, R.P. Ellwood, Measuring initial enamel erosion with quantitative light-induced fluorescence and optical coherence tomography: an in vitro validation study, Caries Res. 48 (2014) 254–262, https://doi.org/10.1159/000354411.
[22] H.-M. Ku, B.-R. Kim, S.-M. Kang, J.-H. Chung, H.-K. Kwon, B.-I. Kim, Detection of early changes in caries lesion using QLF-D and OCT, J. Korean Acad. Oral Heal. 38 (2014) 10–16, https://doi.org/10.11149/jkaoh.2014.38.1.10.
[23] J. Gomez, C. Zakian, S. Salsone, S.C.S. Pinto, A. Taylor, I.A. Pretty, R. Ellwood, In vitro performance of different methods in detecting occlusal caries lesions, J. Dent. 41 (2013) 180–186, https://doi.org/10.1016/j.jdent.2012.11.003.
[24] M. Machoy, J. Seeliger, L. Szyszka-Sommerfeld, R. Koprowski, T. Gedrange, K. Woźniak, The use of optical coherence tomography in dental diagnostics: a state-of-the-art review, J. Healthc. Eng. 2017 (2017) 1–31, https://doi.org/10.1155/2017/7560645.
[25] P. Mylonas, R.S.S. Austin, R. Moazzez, A. Joiner, D.W.W. Bartlett, In vitro evaluation of the early erosive lesion in polished and natural human enamel, Dent. Mater. 34 (2018) 1391–1400, https://doi.org/10.1016/j.dental.2018.06.018.
[26] K. Watanabe, T. Tanaka, K. Maki, H. Nakashima, S. Watanabe, Amount of calcium elution and eroded lesion depth in bovine enamel derived from single short time immersion in carbonated soft drink in vitro, Open J. Stomatol. 05 (2015) 80–86, https://doi.org/10.4236/ojst.2015.53012.
[27] K.R. Stenhagen, L.H. Hove, B. Holme, S. Taxt-Lamolle, A.B. Tveit, Comparing different methods to assess erosive lesion depths and progression in vitro, Caries Res. 44 (2010) 555–561, https://doi.org/10.1159/000321536.
[28] C. Ganss, A. Lussi, J. Klimek, Comparison of calcium/phosphorus analysis, longitudinal microradiography and profilometry for the quantitative assessment of erosive demineralisation, Caries Res. 39 (2005) 178–184, https://doi.org/10.1159/000084795.
[29] M. Eisenburger, J. Hughes, N.X. West, K.D. Jandt, M. Addy, Ultrasonication as a method to study enamel demineralisation during acid erosion, Caries Res. 34 (2000) 289–294, https://doi.org/10.1159/000016604.
[30] M.J.F. Hookham, R.J.M. Lynch, D.P. Naughton, Characterisation of mineral loss as a function of depth using confocal laser scanning microscopy to study erosive lesions in enamel: A novel non-destructive image processing model, J. Dent. 99 (2020) 103402, https://doi.org/10.1016/j.jdent.2020.103402.
[31] M. Fontana, Y. Li, A.J. Dunipace, T.W. Noblitt, G. Fischer, B.R. Katz, G.K. Stookey, Measurement of enamel demineralization using microradiography and confocal microscopy, Caries Res. 30 (1996) 317–325, https://doi.org/10.1159/000262337.
[32] A. Lussi, N. Schlueter, E. Rakhmatullina, C. Ganss, Dental erosion – an overview with emphasis on chemical and histopathological aspects, Caries Res. 45 (2011) 2–12, https://doi.org/10.1159/000325915.
[33] R.P. Shellis, M.E. Barbour, S.B. Jones, M. Addy, Effects of pH and acid concentration on erosive dissolution of enamel, dentine, and compressed hydroxyapatite, Eur. J. Oral Sci. 118 (2010) 475–482, https://doi.org/10.1111/j.1600-0722.2010.00763.x.
[34] F. Lippert, R.J.M. Lynch, Comparison of knoop and vickers surface microhardness and transverse microradiography for the study of early caries lesion formation in human and bovine enamel, Arch. Oral Biol. 59 (2014) 704–710, https://doi.org/10.1016/j.archoralbio.2014.04.005.
[35] F. Mullan, R.S. Austin, C.R. Parkinson, A. Hasan, D.W. Bartlett, Measurement of surface roughness changes of unpolished and polished enamel following erosion, PLoS One 12 (2017) e0182406, https://doi.org/10.1371/journal.pone.0182406.
[36] J.C. Elliott, General chemistry of the calcium orthophosphates, Stud. Inorg. Chem. 18 (1994) 1–62, https://doi.org/10.1016/B978-0-444-81582-8.50006-7.
[37] R.P. Shellis, B.R. Heywood, F.K. Wahab, Formation of brushite monetite and whitlockite during equilibration of human enamel with acid solutions at 37oC, Caries Res. 31 (1997) 71–77, https://doi.org/10.1159/000262377.
[38] M.J. Larsen, S.J. Jensen, Stability and mutual conversion of enamel apatite and brushite at 20 °C as a function of pH of the aqueous phase, Arch. Oral Biol. 34 (1989) 963–968, https://doi.org/10.1016/0003-9969(89)90053-8.
[39] X.J. Gao, J.C. Elliott, P. Anderson, Scanning and contact microradiographic study of the effect of degree of saturation on the rate of enamel demineralization, J. Dent. Res. (1991), https://doi.org/10.1177/00220345910700100401.
[40] R.J.M. Lynch, U. Mony, J.M. ten Cate, The effect of fluoride at plaque fluid concentrations on enamel de- and remineralisation at low pH, Caries Res. 40 (2006) 522–529, https://doi.org/10.1159/000095652.
[41] L. Wang, G.H. Nancollas, Calcium orthophosphates: crystallization and dissolution, Chem. Rev. 108 (2008) 4628–4669, https://doi.org/10.1021/cr0782574.
[42] K. Kuroda, M. Okido, Hydroxyapatite coating of titanium implants using hydroprocessing and evaluation of their osteoconductivity, Bioinorg. Chem. Appl. 2012 (2012) 1–7, https://doi.org/10.1155/2012/730693.
[43] R.J.M. Lynch, J.M. ten Cate, The Effect of Lesion Characteristics at Baseline on Subsequent De- and Remineralisation Behaviour, Caries Res. 40 (2006) 530–535, https://doi.org/10.1159/000095653.
[44] F. Lippert, A. Butler, R.J.M. Lynch, A.T. Hara, Effect of fluoride, lesion baseline severity and mineral distribution on lesion progression, Caries Res. 46 (2012) 23–30, https://doi.org/10.1159/000334787.
[45] E. Heurich, M. Beyer, K.D. Jandt, J. Reichert, V. Herold, M. Schnabelrauch, B. W. Sigusch, Quantification of dental erosion-a comparison of stylus profilometry and confocal laser scanning microscopy (CLSM), Dent. Mater. 26 (2010) 326–336, https://doi.org/10.1016/j.dental.2009.12.001.
[46] A.M.A. Maia, C. Longbottom, A.S.L. Gomes, J.M. Girkin, Enamel erosion and prevention efficacy characterized by confocal laser scanning microscope, Microsc. Res. Tech. 77 (2014) 439–445, https://doi.org/10.1002/jemt.22364.
[47] F. Mullan, D. Bartlett, R.S. Austin, Measurement uncertainty associated with chromatic confocal profilometry for 3d surface texture characterization of natural human enamel, Dent. Mater. 33 (2017) e273–e281, https://doi.org/10.1016/j.dental.2017.04.004.